Springer manuscript No.
(will be inserted by the editor)

Robust Multiphase Topology Optimization Accounting for Manufacturing Uncertainty via Stochastic Collocation

Vahid Keshavarzzadeh · Kai A. James

Received: date / Accepted: date

Abstract This paper presents a computational framework for multimaterial topology optimization under uncertainty. We combine stochastic collocation with design sensitivity analysis to facilitate robust design optimization. The presence of uncertainty is motivated by the induced scatter in the mechanical properties of candidate materials in the additive manufacturing process. The effective elastic modulus in each finite element is obtained by an interpolation scheme which is parameterized with three distinct elastic moduli corresponding to the available design materials. The parametrization enables the SIMP-style penalization of intermediate material properties, thus ensuring convergence to a discrete manufacturable design. We consider independent random variables for the elastic modulus of different materials and generate designs that minimize the variability in the performance, namely structural compliance. We use a newly developed quadrature rule, *designed quadrature* to compute statistical moments with reduced computational cost. We show our approach on numerical benchmark problems of linear elastic continua where we demonstrate the improved performance of robust designs compared to deterministic designs. We provide the MATLAB implementation of our approach.

Keywords Multimaterial Topology Optimization · Additive Manufacturing · Robust Design Optimization · Stochastic Collocation

1 Introduction

Topology optimization is a computational tool for the distribution of given material resources within a specified spatial domain to achieve the maximum performance, typically maximum stiffness. This technique was originally introduced by Bendsøe and Kikuchi [1], who sought to optimize the structural layout, instead of structural boundaries as is done in shape optimization. In the early stages, the main focus of topology optimization was on solid mechanics [2], however this method has been significantly developed and extended throughout the decades to various fields such as heat conduction, fluid dynamics, and multi-physics problems [3–8].

Topology optimization researchers have long recognized the importance of accounting for the manufacturing process during design optimization, in order to allow the algorithms to access to full feasible design space efficiently. Early research on this topic focused on defining appropriate design constraints that would ensure that the resulting optimized designs remained feasible given the limitations of the intended manufacturing process. Early efforts to solve this problem include a 2012 study by Guest and Zhu in which they used projection methods to enforce geometry specifications corresponding to the casting and milling manufacturing processes [9]. More recently, a 2016 paper by Vatanabe *et al.* presented a unified projection-based method for generating optimized designs that are compatible with a variety of manufacturing processes including extrusion, turning, casting, forging and rolling [10].

Vahid Keshavarzzadeh
Department of Mechanical Science and Engineering, University of Illinois at Urbana-Champaign
E-mail: vkeshava@illinois.edu

Kai A. James
Department of Aerospace Engineering, University of Illinois at Urbana-Champaign
E-mail: kaijames@illinois.edu

In contrast to casting and milling, additive manufacturing (AM) enables the fabrication of very complex, intricate geometries. This capability provides designers with nearly full access to the space of potential designs, however each AM process comes with its own set of specific limitations that must be considered when developing AM-compatible topology optimization algorithms [11]. One of the primary challenges when 3D printing topology optimized designs is the need for postprocessing in order to convert a rasterized representation of the design geometry into a CAD model that can be prototyped. Zegard and Paulino have introduced an algorithm and software tool for automating this process and for ensuring the connectedness of the design geometry using a novel convolution (weighting) function for filtering densities [12]. Another pervasive challenge in design for additive manufacturing is the issue of overhang. Because 3D printed parts are built layer-by-layer, geometries that have large regions of overhang require the use of extensive support material to be used as scaffolding. It has been estimated that the printing of support material accounts for 40 - 70% additive manufacturing costs [11], therefore, reducing the amount of support material required to manufacture a part can significantly reduce both the time and cost of the manufacturing process. A large number of studies have investigated various approaches to addressing this issue using topology optimization [13–15], with several authors implementing projection-based approaches [16–19] similar to those mentioned above.

Other researchers have sought to develop algorithms that optimally exploit the multimaterial capability of various AM technologies. In a 2014 paper, Gaynor *et al.* presented a SIMP-style multimaterial topology optimization method for 3D printed mechanisms [20]. In this approach, the material properties were computed as a superposition of the respective properties the various design material options. The method was validated experimentally by prototyping a series of multimaterial compliant mechanisms using the Polyjet 3D printing process. More recently, Conlan-Smith and James presented a multiphase topology optimization method for the design of functionally graded compliant mechanisms [21]. Here, they introduced a novel material interpolation scheme in which the material properties could vary continuously within a set of bounds corresponding to two base material phases. The co-author, James, also published a 2018 paper in which he introduced a method for performing multimaterial topology optimization in which the algorithm optimally selects from a suite of candidate materials. This method was designed to accommodate AM technologies in which the printer offers a wide selection of material options, but can include only two or three of these materials within a single part.

The majority of existing research on design for AM and multimaterial topology optimization focuses on deterministic analysis and optimization. However, the design performance varies due to inherent uncertainties in different parameters such as loading, boundary conditions, material properties and geometry. The additive manufacturing process presents unique challenges with regard to robust design, since AM methods contain multiple unique sources of uncertainty [22] that can diminish the performance of the manufactured part. Stochastic design methods tackle this deficiency by incorporating uncertainty analysis in the optimization process. Such methods fall into two main categories: robust design optimization (RDO) [23–26], which minimizes the performance variation, and reliability based design optimization (RBDO) [27, 28] which constrains the failure probability (or failure events). The computational complexity is the outstanding challenge in these approaches, which require a considerable number of expensive simulations to capture variations in the response function.

In this work we present a systematic topology optimization approach which considers the scatter in the material properties of candidate materials within an AM process. We present our approach in the context of density-based topology optimization, and focus on RDO to minimize the performance variability in the optimal design. In particular we take advantage of the stochastic collocation method, which provides a generic tool for estimation of statistical moments and their sensitivities [29]. The key ingredient of the stochastic collocation method is the numerical integration strategy for multivariate functions. *Sparse grids* are a widely used tool for such integration tasks, as they provide a level of computational efficiency that exceeds that of other integration approaches such as Monte Carlo or the standard tensor product of univariate Gaussian quadrature [30]. In this work we adopt a newly developed quadrature rule, called *designed quadrature*, for integration of multivariate functions, which has been shown to be superior to sparse grids integration [31].

The merits of our contribution are twofold. First, it is one of the first few papers which consider a robust design formulation for multimaterial topology optimization. It is noteworthy to mention some of the similar works in the literature at this juncture. In [32] robust concurrent optimization of material and structure under unknown-but-bounded load uncertainties is investigated in a multi-scale framework. Authors in [33] study the topology optimization for mechanical systems with hybrid material and geometric uncertainties using a memory-less transformation of random fields. In [34] authors present an approach for robust topology optimization of continuum structures under loading and material uncertainties based on an optimality criterion obtained from the stochastic linear elasticity problem. In [35] authors use stochastic collocation combined with full tensor product grid and Smolyak sparse grid to transform the robust formulation into a weighted multiple loading deterministic problem at the collocation points. Authors in [36] propose a density-based approach in conjuction with a univariate dimension-reduction method combined with Gauss-type quadrature sampling

for robust multimaterial topology optimization. While these works consider a similar problem to the one we consider in this paper we believe our contribution is the first one which provides a systematic and rigorous way for robust multimaterial topology optimization. In particular our approach combines two well-established methods: 1) a SIMP-style approach for multimaterial topology optimization and 2) a stochastic collocation approach for uncertainty analysis. Second, we successfully utilize the designed quadrature capability in approximating statistical moments with reduced cost within a robust design framework. We discuss the key steps of the computational procedure for robust multiphase topology optimization in detail. In addition we provide the MATLAB code which computes the quantities of interest such as the statistical moments of compliance, volume and mechanical advantage for multiphase continua, which can be found in the repository whose Uniform Resource Locator (URL) is given in [37]. All gradient-based optimization is performed using the *method of moving asymptotes* (MMA), details of which can be found in [38]. Part of our implementation leverages the fast routine for FEA in [39], and the rest of our implementation uses MATLAB vectorization, which together comprise an efficient code for optimization under uncertainty.

The rest of paper is organized as follows. Section 2 briefly describes the topology optimization method including its deterministic and robust forms. The details of multimaterial parameterization with uncertainty and sensitivity analyses are presented in Section 3. Section 4 presents numerical results for topology optimization of linear elastic structures and a heat sink which involves a similar boundary value problem. Finally, Section 5 contains the concluding remarks.

2 Topology Optimization: Deterministic and Robust

2.1 Notation and Setup

- We use bold characters to denote multivariate quantities such as matrices and vectors e.g. $\boldsymbol{x}$ indicates a vector of variables in the domain of a multivariate function.
- We denote sets with uppercase letters e.g. Ω is a set of events (or event space).
- We show the index for variable coordinates in multivariate quantities via subscripts $._i$ and the sample realization of such quantities via superscripts $.^{(j)}$. For example $y_i^{(j)}$ is the (j)-th realization of variable y_i.
- Suppose data $(y_1^{(j)}, y_2^{(j)}, \ldots, y_d^{(j)})_{j=1}^n$ is given. Each datum is sampled from a joint distribution on a compact space $(y_1^{(j)}, y_2^{(j)}, \ldots, y_d^{(j)}) \in \Omega \subset \mathbb{R}^d$, where $\Omega = \mathcal{Y}_1 \times \ldots \times \mathcal{Y}_d$ is a tensor product space with $\mathcal{Y}_k \subset \mathbb{R}$. The joint distribution is denoted by $\pi(\boldsymbol{y}) = \pi_{y_1} \times \ldots \times \pi_{y_d}$, where π_{y_k} is the marginal distribution of variable y_k.

We solve a robust design optimization problem, which is formulated based on the statistical moments of volume and compliance cf. Figure 1. The uncertainty is considered in the nominal elastic modulus of candidate materials in multimaterial topology optimization. Our stochastic analysis at each design iterate is comprised of several deterministic simulations on particularly designed quadrature points to compute the statistical moments of compliance, volume and their sensitivities cf. Section 2. We also present a numerical example considering thermal compliance with multiple materials with uncertain thermal conductivity. Our deterministic simulations follow a particular multimaterial algorithm [40], which will be briefly described in Section 3.

2.2 Deterministic Topology Optimization

The topology optimization method distributes a given material resource within a prescribed physical domain to maximize structural performance. It is a constrained optimization problem in which typically the objection function is the structural compliance and the constraint is the mass (or volume) of material. The optimization problem in its general form can be written as

$$\begin{aligned} &\min_{\boldsymbol{\rho}} \; g_0(\boldsymbol{\rho}) \\ &\text{subject to } g_i(\boldsymbol{\rho}) = 0 \quad i = 1, \ldots, n_e \\ &\qquad\qquad \tilde{g}_i(\boldsymbol{\rho}) \leq 0 \quad i = 1, \ldots, n_i \end{aligned} \tag{1}$$

where g_0 is the objective function, g_i and $\tilde{g}_i$ are sets of equality and inequality constraints and $\boldsymbol{\rho}$ is the design parameter, which, in this article, represents the volume fraction (or relative material density) of each finite element. The elastic

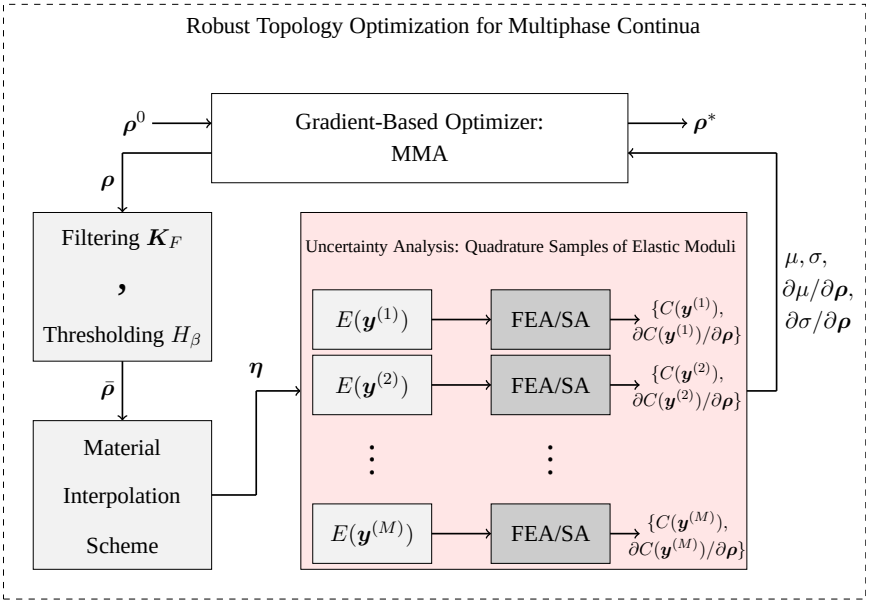

Fig. 1: Flowchart for robust multiphase topology optimization. FEA ans SA stand for Finite Element Analysis and Sensitivity Analysis respectively.

response of the structure is characterized by governing equation, which is typically obtained and solved via finite element discretization of the boundary value problem shown below.

$$\begin{cases} \nabla.\boldsymbol{\sigma}(\boldsymbol{x}) + \mathbf{b}(\boldsymbol{x}) = 0 & \forall \boldsymbol{x} \in D \\ \boldsymbol{\sigma}(\boldsymbol{x})\mathbf{n} = n(\boldsymbol{x}) & \forall \boldsymbol{x} \in \Gamma_N \\ \boldsymbol{u}(\boldsymbol{x}) = 0 & \forall \boldsymbol{x} \in \Gamma_D \end{cases} \tag{2}$$

where the physical domain $D \subset \mathbb{R}^d$, $d = 2, 3$ is a bounded and Lipschitz continuous domain with two sets of Dirichlet Γ_D and Neumann Γ_N boundary conditions where $\Gamma_N \cap \Gamma_D = \emptyset$, cf. Figure 2. The above governing equations are

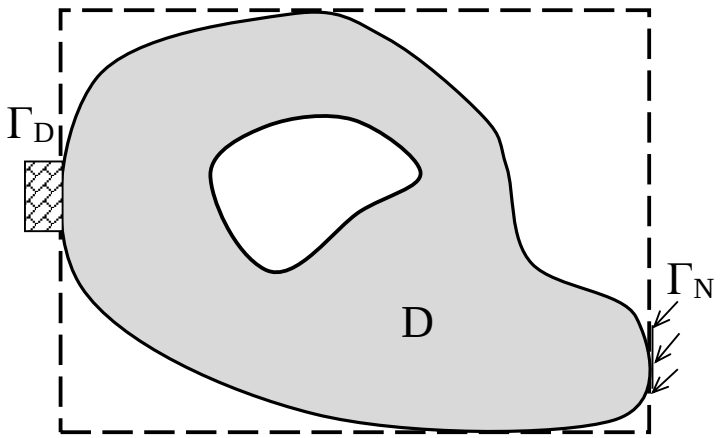

Fig. 2: Schematic representation of the spatial domain associated with the topology optimization problem

presented in the form of a linear elliptic partial differential equation

$$\begin{cases} -\nabla.(\mathbb{C}(\boldsymbol{x})\nabla \boldsymbol{u}(\boldsymbol{x})) = f(\boldsymbol{x}) & \forall \boldsymbol{x} \in D \\ \boldsymbol{u}(\boldsymbol{x}) = 0 & \forall \boldsymbol{x} \in \partial D \end{cases} \tag{3}$$

where $\mathbb{C}$ is the elasticity matrix. We note that the union of the spatial domain with the traction boundary $\{D \cup D_N\}$ is denoted by D, and ∂D denotes the Dirichlet boundary condition.

As standard procedures in density based topology optimization, we process the design variables throughout the optimization iterations by filtering the densities to impose a minimum length scale [41] and thresholding them to generate more distinct interfaces [42]. The filtered volume fractions are expressed via the cone Kernel K_F as

$$\hat{\rho}(\boldsymbol{x}) = \frac{\int_{R_F} K_F(\boldsymbol{x}, \boldsymbol{x}')\rho(\boldsymbol{x}')d\boldsymbol{x}'}{\int_{R_F} K_F(\boldsymbol{x}, \boldsymbol{x}')d\boldsymbol{x}'} \tag{4}$$

where R_F is the application area of the filter defined by r_{min} and K_F is denoted by

$$K_F(\boldsymbol{x}, \boldsymbol{x}') = \begin{cases} r_{min} - |\boldsymbol{x} - \boldsymbol{x}'| & \text{if } |\boldsymbol{x} - \boldsymbol{x}'| \leq r_{min} \\ 0 & \text{if } |\boldsymbol{x} - \boldsymbol{x}'| > r_{min} \end{cases} \tag{5}$$

The Heaviside step function is used to ideally threshold the filtered volume fractions to ρ_{min} and 1 where ρ_{min} is the lower bound for volume fractions i.e.

$$\bar{\rho} = H(\hat{\rho} - \rho_{min}) = \begin{cases} 1 & \text{if } \hat{\rho} \geq \rho_{min}, \\ \rho_{min} & \text{if } \hat{\rho} = \rho_{min}. \end{cases} \tag{6}$$

However, to facilitate gradient-based optimization, a smooth approximation of step function is used [42],

$$\bar{\rho} = H_\beta(\hat{\rho}) = 1 - e^{-\beta\hat{\rho}} + \hat{\rho}e^{-\beta}, \tag{7}$$

where the lower bound ρ_{min} is adjusted for the selected β such that $\rho_{min} = H_\beta(\rho_{min})$. In this approximation, β controls the smoothness of transition from zero to one i.e. $\lim_{\beta\to\infty} H_\beta(\hat{\rho}) = H(\hat{\rho} - \rho_{min})$.

We finally use the standard Solid Isotropic Material with Penalization (SIMP) method to penalize intermediate volume fractions [43, 44] i.e. we compute the global stiffness matrix $\boldsymbol{K}$ by using the processed (thresholded-filtered) volume fractions $\bar{\rho}$,

$$\boldsymbol{K} = \sum_{i=1}^{n_e} \bar{\rho_i}^\kappa \boldsymbol{K}_i, \tag{8}$$

where n_e is the number of elements, $\kappa = 3$ is the penalization parameter and $\boldsymbol{K}_i$ is the nominal element i stiffness matrix.

2.3 Robust Topology Optimization

We formulate the optimization problem with respect to the statistical moments of compliance and volume in robust topology optimization,

$$\begin{aligned} \min_{\boldsymbol{\rho}} \; & Q(\lambda) = \mu(\boldsymbol{\rho}) + \lambda\sigma(\boldsymbol{\rho}) \\ \text{subject to } & \mathbb{E}[V(\boldsymbol{\rho})] \leq \bar{V} \\ & \rho_{min} \leq \boldsymbol{\rho} \leq 1, \end{aligned} \tag{9}$$

where μ and σ are mean and standard deviation of compliance, $\mathbb{E}$ is the expected value operator and λ is the weight factor for the standard deviation in robust design. We note that the compliance is dependent on the medium's elasticity. In this paper we also formulate the optimization problem with a resource constraint based on the amount of material that can appear in the structure. We in particular assume that stiffer materials are more heavy, or more costly to procure and therefore they are weighted more heavily in the resource constraint cf. Equation (16). Therefore, the randomness in material resource and compliance is due to the randomness in the uncertain parameters that influence the elasticity of the medium.

Now Let $(\Omega, \mathcal{A}, \mathcal{P})$ be a complete probability space, where Ω is the event space, $\mathcal{A} \subset 2^{\Omega}$ is the σ-algebra, and $\mathcal{P}$ is the probability measure. Considering the spatial bounded domain D with boundary ∂D we are interested in the following problem: find a stochastic function, $\boldsymbol{u} \equiv \boldsymbol{u}(\boldsymbol{y}, \boldsymbol{x}) : \Omega \times D \to \mathrm{R}$, such that for $\mathcal{P}$-almost everywhere $\boldsymbol{y} \in \Omega$, the following equation (the parametric counterpart of Equation (3)) holds:

$$\begin{cases} \nabla.(\mathbb{C}(\boldsymbol{y}, \boldsymbol{x})\nabla \boldsymbol{u}(\boldsymbol{y}, \boldsymbol{x})) = f(\boldsymbol{x}) & \forall (\boldsymbol{y}, \boldsymbol{x}) \in \Omega \times D \\ \boldsymbol{u}(\boldsymbol{y}, \boldsymbol{x}) = 0 & \forall (\boldsymbol{y}, \boldsymbol{x}) \in \Omega \times \partial D \end{cases} \tag{10}$$

where $\boldsymbol{y} = \{y_i\}_{i=1}^{d}$ denotes the vector of parameters (or random variables), $\mathbb{C}$ is again the elasticity matrix parameterized with the random variables and d is the number of random variables. Approximating the stochastic function via Lagrange polynomials $L_k(\boldsymbol{y})$ such that

$$\hat{\boldsymbol{u}}(\boldsymbol{y}, \boldsymbol{x}) = \sum_{k=1}^{M} \boldsymbol{u}(\boldsymbol{y}^{(k)}, \boldsymbol{x}) L_k(\boldsymbol{y}) \tag{11}$$

where M is the number of collocation points and denoting the left hand side in Equation (10) (top) as $\mathcal{L}(\boldsymbol{u}) = \nabla.(\mathbb{C}(\boldsymbol{y}, \boldsymbol{x})\nabla \boldsymbol{u}(\boldsymbol{y}, \boldsymbol{x}))$, the stochastic collocation approach solves the following residuals

$$\mathcal{R}(\hat{\boldsymbol{u}}(\boldsymbol{y}))|_{\boldsymbol{y}^{(k)}} = 0 \quad \forall k = 1, \ldots, M \tag{12}$$

where $\mathcal{R}(\hat{\boldsymbol{u}}) = \mathcal{L}(\hat{\boldsymbol{u}}) - f$ [29]. Using the property of Lagrange polynomials this approach is equivalent to solving the deterministic elliptic PDE problem

$$\begin{cases} \nabla.(\mathbb{C}(\boldsymbol{y}^{(k)}, \boldsymbol{x})\nabla \boldsymbol{u}(\boldsymbol{y}^{(k)}, \boldsymbol{x})) = f(x) & \forall \boldsymbol{x} \in D \\ \boldsymbol{u}(\boldsymbol{y}^{(k)}, \boldsymbol{x}) = 0 & \forall \boldsymbol{x} \in \partial D \end{cases} \tag{13}$$

on collocation points $\{\boldsymbol{y}^{(k)}\}_{k=1}^{M}$ to find coefficients $\boldsymbol{u}(\boldsymbol{y}^{(k)}, \boldsymbol{x})$. Once these coefficients are obtained, computing the statistical moments of the solution (e.g. the expected value) is straightforward:

$$\mathbb{E}[\hat{\boldsymbol{u}}(\boldsymbol{x})] = \sum_{k=1}^{M} \boldsymbol{u}(\boldsymbol{y}^{(k)}, \boldsymbol{x}) \int_{\Omega} L_k(\boldsymbol{y}) \pi(\boldsymbol{y}) d\boldsymbol{y} \tag{14}$$

In this equation π is the multivariate probability density function. The evaluation of the above integral is typically performed via quadrature rules i.e. $\int_{\Omega} f(\boldsymbol{y})\pi(\boldsymbol{y})d\boldsymbol{y} = \sum_{k=1}^{M} f(\boldsymbol{y}^{(k)})w^{(k)}$ where $w^{(k)}$ are quadrature weights. Using a quadrature rule, Equation (14) reduces to

$$\mathbb{E}[\hat{\boldsymbol{u}}(\boldsymbol{x})] = \sum_{k=1}^{M} \boldsymbol{u}(\boldsymbol{y}^{(k)}, \boldsymbol{x}) w^{(k)} \tag{15}$$

It is clear that the accuracy of statistical moments depends on the quadrature rule, and particularly the number of quadrature points. A common integration rule for multivariate functions is *Sparse Grids*, which provides a requisite accuracy with smaller cost (i.e. a smaller number of nodes) compared to other integration rules such as the standard tensor product of Gaussian quadratures. However, Sparse Grids suffer from negative weights which in some cases may yield erroneous results. In addition, the number of points is not optimal since the node coordinations are dictated by the univariate Gaussian quadrature rule[45, 46].

In this work we adopt a newly introduced quadrature rule, designed quadrature [31] which circumvents these challenges. Designed quadrature provides a set of optimized quadrature nodes with positive weights which are considerably fewer than Sparse Grids nodes and hence is more efficient for stochastic collocation computations.

3 Multimaterial Topology Optimization

3.1 Parametrization of the Effective Elastic Modulus

The multiphase design approach selects a particular solid phase with elastic modulus E_i from multiple solid phases $\{E_i\}_{i=1}^{n_m}$ at each element where n_m is the number of candidate solid materials. [1]This formulation allows design of

[1] The total number of phases is $n_m + 1$, which includes void phase.

structures with optimal material properties in local regions. In its basic form, the multiphase compliance minimization subject to a mass constraint is expressed as an integer program.

$$\begin{aligned} &\min_{\boldsymbol{\eta}} C(E(\boldsymbol{x})) \\ &\text{subject to } E(\boldsymbol{x}) = \sum_{i=1}^{n_m+1} E_i \eta_i(\boldsymbol{x}), \\ &\sum_{i=1}^{n_m+1} \eta_i(\boldsymbol{x}) = 1 \qquad \forall \boldsymbol{x} \in D, \\ &\boldsymbol{\eta}(\boldsymbol{x}) \in \{0,1\}^{n_m+1} \qquad \forall \boldsymbol{x} \in D, \\ &\textstyle\int_D E(\boldsymbol{x}) d\boldsymbol{x} \leq \bar{E}. \end{aligned} \tag{16}$$

where $\boldsymbol{\eta} = \{\eta_i\}_{i=1}^{n_m+1}$ is a set of integer numbers taking the binary values of 0 and 1 which parameterize the effective elastic modulus $E(\boldsymbol{x})$, and $\bar{E}$ is the upper limit for total elastic modulus within the structure (equivalent to the total mass or volume).

The problem in this present form is a combinatorial problem similar to the original topology optimization problem. To relax these integer constraints we adopt a similar approach to SIMP and interpolate the effective elastic modulus from discrete elastic modulus values via smooth functions. In particular we follow the shape function approach in [40] for three-phase design which we describe here briefly.

Similarly to standard density-based topology optimization, which uses a design parameter ρ_i for each element we consider two design parameters $\rho_i,\ i = 1,2$ per element and apply the filtering and thresholding operators on both variables i.e. $\rho_i \rightarrow \hat{\rho}_i \rightarrow \bar{\rho}_i,\ i = 1,2$ cf. Section 2.2, to find processed design variables $\bar{\rho}_1, \bar{\rho}_2$. We then compute the activation functions η_i (smooth counterparts of integer numbers in Equation (16)) via

$$\begin{aligned} \eta_1 &= \bar{\rho}_1^p \bar{\rho}_2^p & \eta_2 &= \bar{\rho}_1^p (1-\bar{\rho}_2)^p \\ \eta_3 &= (1-\bar{\rho}_1)^p \bar{\rho}_2^p & \eta_4 &= (1-\bar{\rho}_1)^p (1-\bar{\rho}_2)^p \end{aligned} \tag{17}$$

where p is a penalization constant used to penalize the intermediate values of $\rho_i \in [0,1]$ similarly to SIMP. The number of activation functions is four which includes the void phase in addition to three material phases. We set the first elastic modulus value as the void phase such that $E_1 = E_{min}$. For instance parameter values $\bar{\rho}_1 = \bar{\rho}_2 = 1$ activate (or model) the void phase i.e. when $\eta_1 = 1$. Note that for $p = 1$ we recover the standard bilinear finite element shape functions. For $p > 1$ these functions are convex with respect to parameters ρ_i which ensures a discrete solution for the optimization problem. Similar to the standard SIMP method, we set $p = 3$ in our numerical examples. Note that in cases where we have more than three solid material candidates, the formulation can be extended by adding additional design parameters for each element. In general, the method can accommodate up to n_m candidate materials with $n_m = 2^{n_p} - 1$, where n_p is the number of design parameters for each finite element. For example, multiplying each of four η_i in Equation (17) with two multipliers $\bar{\rho}_3^p$ and $(1-\bar{\rho}_3)^p$ where $\bar{\rho}_3$ denotes the third design parameter, results in eight activation functions η_i which parameterize seven solid and one void phases. Now that we have parameterized the design domain with smooth functions, we solve the relaxed version of (16) with constraints $\rho_1, \rho_2 \in [0,1]$ replacing $\boldsymbol{\eta}(\boldsymbol{x}) \in \{0,1\}^{n_m+1}$ via the Method of Moving Asymptotes (MMA). MMA is a general nonlinear programming method which generates and solves a sequence of convex subproblems with improved feasible (or almost feasible) solutions of the subject problem. Due to its generality and flexibility it has been widely used in the field of structural optimization [38].

3.2 Adjoint Sensitivity Analysis

In order to use efficient gradient-based optimizers we need to compute design sensitivities. The subject of sensitivity analysis has been discussed extensively in the literature[47], however we briefly discuss sensitivity analysis for a particular quantity of interest, the mechanical advantage which will be used in one of our numerical examples for designing a compliant mechanism.

The finite element equilibrium equations can be partitioned and expressed in terms of free (f) and constrained (c) degrees of freedom in the residual form

$$\boldsymbol{R} = \begin{bmatrix} \boldsymbol{R}_f \\ \boldsymbol{R}_c \end{bmatrix} = \begin{bmatrix} \boldsymbol{K}_{ff} & \boldsymbol{K}_{fc} \\ \boldsymbol{K}_{cf} & \boldsymbol{K}_{cc} \end{bmatrix} \begin{bmatrix} \boldsymbol{u}_f \\ \boldsymbol{u}_c \end{bmatrix} - \begin{bmatrix} \boldsymbol{F}_f \\ \boldsymbol{F}_c \end{bmatrix} = \begin{bmatrix} \boldsymbol{0} \\ \boldsymbol{0} \end{bmatrix} \tag{18}$$

where in particular R_f and R_c are the residuals of the static equilibrium equation associated with free and constrained degrees of freedom. To perform adjoint sensitivity analysis we express the quantity of interest Q in the augmented Lagrangian form

$$\mathcal{Q}(\boldsymbol{u}_f, \boldsymbol{F}_c, \boldsymbol{\rho}) = Q(\boldsymbol{u}_f, \boldsymbol{F}_c, \boldsymbol{\rho}) + \boldsymbol{\lambda}_f^T \boldsymbol{R}_f(\boldsymbol{u}_f, \boldsymbol{F}_c, \boldsymbol{\rho}) + \boldsymbol{\lambda}_c^T \boldsymbol{R}_c(\boldsymbol{u}_f, \boldsymbol{F}_c, \boldsymbol{\rho}). \tag{19}$$

Now differentiating the augmented Lagrangian with respect to $\boldsymbol{\rho}$ and using the chain rule results in appearance of implicit derivatives $d\boldsymbol{u}_f/d\boldsymbol{\rho}$ and $d\boldsymbol{F}_c/d\boldsymbol{\rho}$ which are annihilated by solving the adjoint equations. The adjoint solution yields

$$\begin{aligned} \boldsymbol{\lambda}_c &= -\frac{\partial Q}{\partial \boldsymbol{F}_c}, \\ \boldsymbol{\lambda}_f &= \boldsymbol{K}_{ff}^{-1} \left[\boldsymbol{K}_{cf} \frac{\partial Q}{\partial \boldsymbol{F}_c} - \frac{\partial Q}{\partial \boldsymbol{u}_f} \right]. \end{aligned} \tag{20}$$

Using the adjoint solutions in Equation (19) the total sensitivity reduces to

$$\frac{d\mathcal{Q}}{d\boldsymbol{\rho}} = \frac{\partial Q}{\partial \boldsymbol{\rho}} + \lambda_f^T \frac{\partial \boldsymbol{R}_f}{\partial \boldsymbol{\rho}} + \lambda_c^T \frac{\partial \boldsymbol{R}_c}{\partial \boldsymbol{\rho}}. \tag{21}$$

For the case where Q is the structural compliance, we can deduce from Equation (20) that $\boldsymbol{\lambda}_c = 0$ and $\boldsymbol{\lambda}_f = -\boldsymbol{K}_{ff}\boldsymbol{F}_f = -\boldsymbol{u}_f$, which yield $\partial C/\partial \boldsymbol{\rho} = -\boldsymbol{u}^T (d\boldsymbol{K}/d\boldsymbol{\rho})\boldsymbol{u}$.

The mechanical advantage is defined as the ratio of the reaction force (or output force $\boldsymbol{F}_{out}$) to the input force $\boldsymbol{F}_{in}$ i.e. $Q_{MA} = \boldsymbol{F}_{out}/|\boldsymbol{F}_{in}|$ which can be simply defined with respect to constrained forces as

$$Q_{MA} = \boldsymbol{\psi}^T \boldsymbol{F}_c \tag{22}$$

where $\boldsymbol{\psi}$ is an index vector with one nonzero entry corresponding to the reaction force's degree of freedom, with magnitude $\|\boldsymbol{\psi}\| = 1/|\boldsymbol{F}_{in}|$. Using these definitions the adjoint solutions are

$$\begin{aligned} \boldsymbol{\lambda}_c &= -\boldsymbol{\psi} \\ \boldsymbol{\lambda}_f &= \boldsymbol{K}_{ff}^{-1} \left[\boldsymbol{K}_{fc} \boldsymbol{\psi} \right] \end{aligned} \tag{23}$$

which subsequently yield the total derivative

$$\frac{\partial Q_{MA}}{\partial \boldsymbol{\rho}} = \left[\boldsymbol{\lambda}_f^T \frac{\partial \boldsymbol{K}_{ff}}{\partial \boldsymbol{\rho}} - \boldsymbol{\psi}^T \frac{\partial \boldsymbol{K}_{cf}}{\partial \boldsymbol{\rho}} \right] \boldsymbol{u}_f \tag{24}$$

3.3 Stochastic Primal and Sensitivity Analyses

The randomness is introduced in the elastic modulus of each candidate solid material as

$$E_i = E_i^0 \exp\left(1 + \delta y_i\right) \tag{25}$$

where E_i^0 is the nominal value for material i, δ is a small number controlling the perturbation around the nominal value and $y_i \sim \mathcal{N}(0, 1)$ is a standard normal random variable [48]. In this paper we have three phases of solid materials; therefore we use a three dimensional quadrature rule for Gaussian variables $\boldsymbol{y} = (y_1, y_2, y_3)$. Corresponding to each quadrature value $\boldsymbol{y}^{(j)}$ which fixes $\{E_i\}_{i=1}^3$, we compute a parametric quantity of interest e.g. compliance $C(\boldsymbol{y}^{(j)})$ and compliance sensitivity $\partial C(\boldsymbol{y}^{(j)})/\partial \boldsymbol{\rho}$ cf. Section 3.2.

We note that in this paper we assume three distinct materials with uncertain elastic moduli. Evidently if the number of material phases increase the computational cost grows factorially as more quadrature points are needed. Using designed quadrature circumvents this issue to some extent however the dependence of computational cost on the number of variables remains significant. It is noted that in practice where the realizations of the uncertain parameter e.g. a

random field for elastic modulus are available, utilizing dimension reduction techniques such as principal component analysis is effective. Once the reduced dimensions are determined a similar quadrature strategy can be used to compute the statistical moments [26].

It is also noted that in this paper we only consider the problem of robust design optimization and do not optimize for failure mitigation. For reliability based design optimization one needs to consider the probability of failure to ensure the structure's safety which requires development of surrogate models. The computation of failure probability and its sensitivity using polynomial surrogates is detailed in [26].

Now that we have the quadrature samples of the primal and sensitivity values we compute their statistical moments similarly to Equation (15). The mean and standard deviation of compliance are

$$\begin{aligned} \mu &= \sum_{k=1}^{M} C(\boldsymbol{y}^{(k)}) w^{(k)}, \\ \sigma &= \left[\sum_{k=1}^{M} C^2(\boldsymbol{y}^{(k)}) w^{(k)} - \mu^2 \right]^{\frac{1}{2}}, \end{aligned} \tag{26}$$

where $w^{(k)}$ is the quadrature weight. Similarly the sensitivities of statistical moments are obtained as

$$\begin{aligned} \frac{\partial \mu}{\partial \boldsymbol{\rho}} &= \sum_{k=1}^{M} \frac{\partial C(\boldsymbol{y}^{(k)})}{\partial \boldsymbol{\rho}} w^{(k)}, \\ \frac{\partial \sigma}{\partial \boldsymbol{\rho}} &= \frac{1}{\sigma} \left[\sum_{k=1}^{M} C(\boldsymbol{y}^{(k)}) \frac{\partial C(\boldsymbol{y}^{(k)})}{\partial \boldsymbol{\rho}} w^{(k)} - \mu \frac{\partial \mu}{\partial \boldsymbol{\rho}} \right]. \end{aligned} \tag{27}$$

Algorithm 1 summarizes the steps of robust multiphase topology optimization for compliance minimization.

Algorithm 1 Robust Multimaterial Topology Optimization

1: Get the unprocessed design variables $\boldsymbol{\rho}$.
2: **for** $k = 1 : M$ **do**
3: Given unprocessed design variables $\boldsymbol{\rho}$ compute processed design variables $\boldsymbol{\rho} \rightarrow \hat{\boldsymbol{\rho}} \rightarrow \bar{\boldsymbol{\rho}}$ cf. Section 2.2.
4: Compute the quadrature sample of elastic moduli $E(\boldsymbol{y}^{(k)})$ cf. Equation (25).
5: Compute the effective elasic modulus $\mathbb{C}(\boldsymbol{y}^{(k)})$ from the interpolation scheme cf. Section 3.1.
6: Compute the quadrature sample of compliance $C(\boldsymbol{y}^{(k)})$ and its sensitivity $\partial C(\boldsymbol{y}^{(k)})/\partial \boldsymbol{\rho}$ cf. Section 3.2.
7: **end for**
8: Compute $\mu, \partial\mu/\partial\boldsymbol{\rho}$ and $\sigma, \partial\sigma/\partial\boldsymbol{\rho}$ cf. Section 3.3.
9: Feed $\mu + \lambda\sigma$ (where λ is a fixed value determined by the designer) and its sensitivity to the optimizer; go to step 1.

4 Numerical Examples

4.1 Modified L-Bracket

In the first example we consider a modified L-bracket used in [49] cf. Figure 3. In all numerical examples, structures are subjected to plane stress conditions and the candidate materials have nominal elastic moduli $E_1^0 = 100\ MPa, E_2^0 = 200\ MPa, E_3^0 = 300\ MPa$, with Poisson's ratio $\nu = 0.3$. The elastic modulus for the void phase is chosen as $E_{void} = 1Pa$. We also add a perturbation $\delta = 0.05$ to the nominal value of the elastic moduli to introduce uncertainty cf. Equation (25) and Figure 4. The optimization starts with uniform design variables $\boldsymbol{\rho} = 0.5$, and the applied force is $f_y = 100\ KN$ on both sides. Taking advantage of symmetry, we model only the half of the domain, which is discretized using 80×80 bilinear square isotropic finite elements.

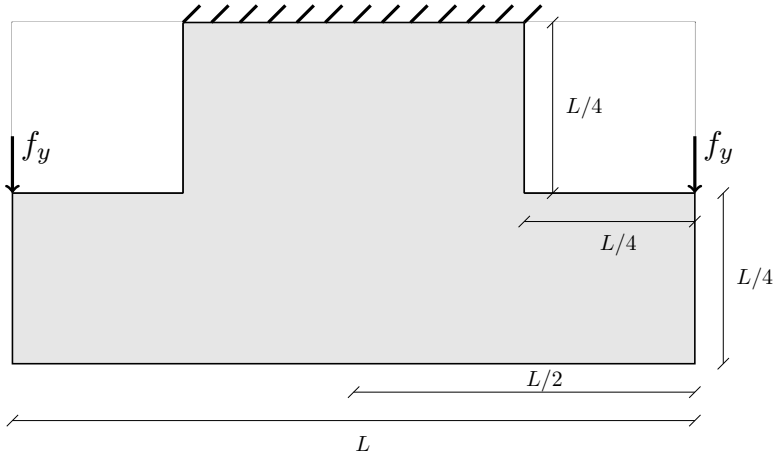

Fig. 3: Design domain for the modified L-bracket.

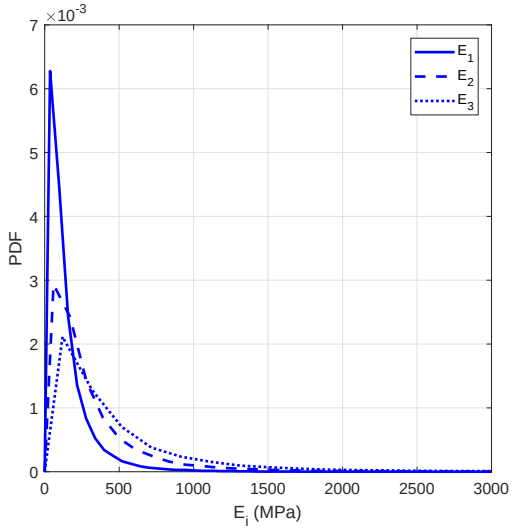

Fig. 4: Distribution of candidate materials' elastic moduli.

We define a normalized parametric volume

$$V(\boldsymbol{y}) = \frac{\sum_{e=1}^{n_e} \sum_{i=1}^{n_m+1} \eta_i(\boldsymbol{x}_e) E_i(\boldsymbol{y})}{n_e E_{max}} \tag{28}$$

where $E_{max} = \max\{E_i^0\}_{i=1}^3$, n_e is the number of elements, and the penalization parameter is set to $p = 1$ for evaluating η_i in this case. The expected value of normalized volume serves as a constraint in the following optimization problem

$$\begin{aligned} &\min_{\boldsymbol{\rho}} \ \mu(\boldsymbol{\rho}) + \lambda\sigma(\boldsymbol{\rho}) \\ &\text{subject to } \mathbb{E}(V(\boldsymbol{\rho})) \leq 0.3, \\ &0 \leq \boldsymbol{\rho} \leq 1. \end{aligned} \tag{29}$$

Figure 5 shows robust designs for different choices of standard deviation weight i.e. $\lambda = 0.01$, $\lambda = 0.1$, $\lambda = 1$. Figure 6 shows the designed quadrature nodes that we use to compute the statistical moments. This quadrature rule integrates

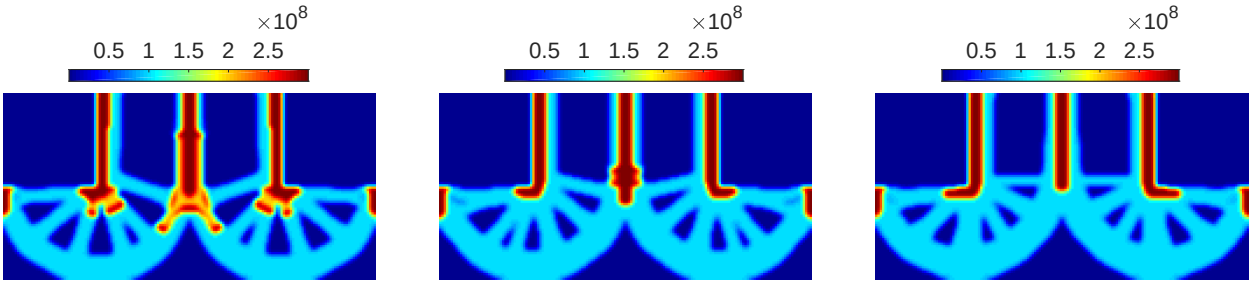

Fig. 5: Optimized material distribution for the modified L-bracket associated with $\lambda = 0.01$ (left), $\lambda = 0.1$ (middle) and $\lambda = 1$ (right). The numbers on the color bar indicate the effective nominal elastic modulus E^0 (in Pa) at each finite element.

standard normal weight function with $d = 3$ variables and total polynomial order $r = 6$. The list of nodes and weights for this quadrature rule is provided in the Appendix.

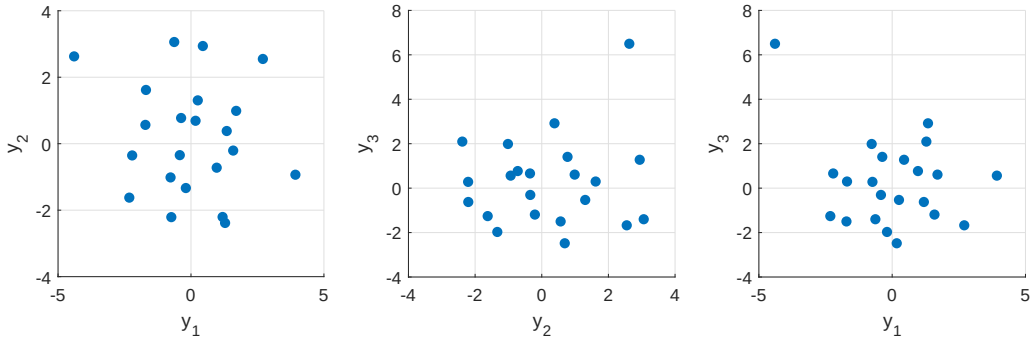

Fig. 6: Designed quadrature nodes for integration of standard normal weight function with $d = 3$ variables and $r = 6$ total polynomial order.

To show the convergence with respect to these points we compare the probability density function (PDF) of compliance associated with the first design in Figure 7 obtained with these points versus the PDF obtained using sparse grids quadrature, with almost equal order. We compute the PDF by developing a Polynomial Chaos Expansion (PCE) [50, 51] on standard normal variables. For a detailed discussion on generating PCEs see [26]. It is evident that the PDFs are in close agreement however designed quadrature is comprised of $M = 22$, points which is significantly smaller than the number of points required for sparse grids quadrature where $M = 39$. Hence designed quadrature reduces the computational cost of the uncertainty analysis by nearly half. We also note that sparse grids nodes have one negative weight associated with the center point $(y_1 = y_2 = y_3 = 0)$ which may cause numerical issues in irregular functions [46].

We compare the robust design (RDO) with a deterministic design (DET) by finding two designs with almost equal volume. Figure 8 shows two designs which are visually distinguishable. We note that the RDO design uses more of the strongest material and both designs converge to a discrete solution. Their performance metrics are listed in Table 1 which clearly shows that the robust design yields a smaller objective value. This result demonstrates that the RDO produces designs whose performance has less mean and less variance and is therefore more robust to uncertainties associated with the manufacturing process. On the other hand, DET design which is obtained from a deterministic optimization using a nominal value for elastic moduli, exhibits larger mean and larger variance when is subjected to stochastic simulations (with uncertain elastic moduli).

To further investigate the accuracy of the quadrature approximate we compute the mean and standard deviation of the compliance associated with robust optimal design using the standard Monte Carlo analysis with 10^4 samples. Table 2 lists the mean and standard deviation which shows close agreement between two approaches.

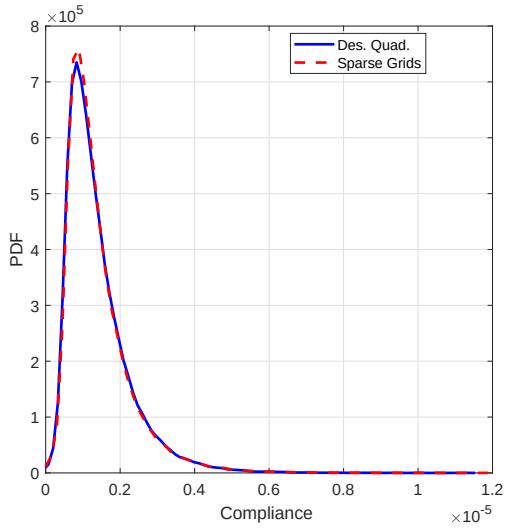

Fig. 7: Comparison of PDFs obtained with designed quadrature and sparse grids using $M = 22$ and $M = 39$ simulations respectively.

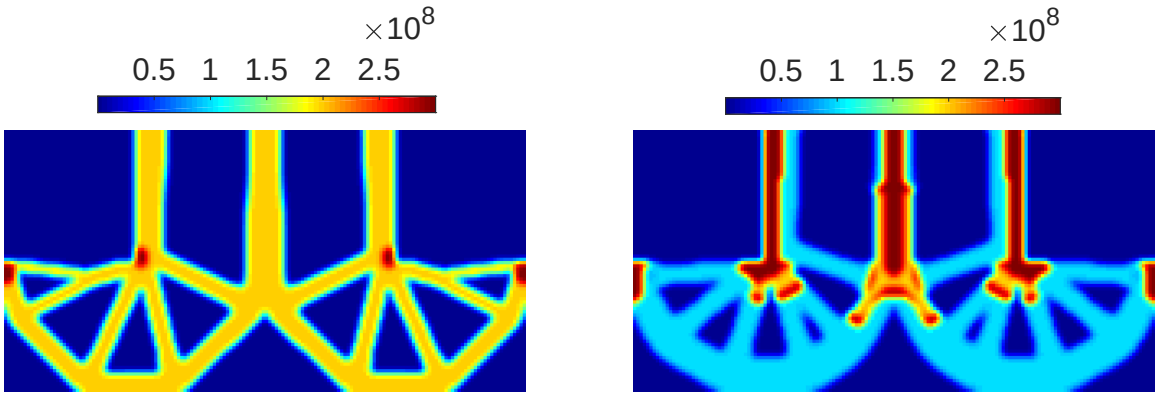

Fig. 8: Topology designs for the modified L-bracket: DET (left), RDO (right).

Table 1: Performance comparison between robust and deterministic designs with $\lambda = 0.01$ for modified L-bracket.

	$\mu\ (N \cdot m)$	$\sigma\ (N \cdot m)$	$\mu + \lambda\sigma\ (N \cdot m)$	$\mathbb{E}(V)$
DET	1.48×10^3	1.30×10^3	1.49×10^3	0.3117
RDO	1.39×10^3	8.54×10^2	1.40×10^3	0.2962

Table 2: Mean and standard deviation of compliance associated with the robust optimal design using designed quadrature and Monte Carlo samples.

	$\mu\ (N \cdot m)$	$\sigma\ (N \cdot m)$
Designed Quadrature	1.39×10^3	8.54×10^2
Monte Carlo	1.37×10^3	8.66×10^2

4.2 Mechanical Inverter

We consider the design of a mechanical inverter, whose boundary conditions are given in Figure 9 to demonstrate the capability of the multiphase approach in designing a structure that combines stiff regions that withstand and transfer the load, with compliant regions for facilitation of motion. In this problem we maximize mechanical advantage subject

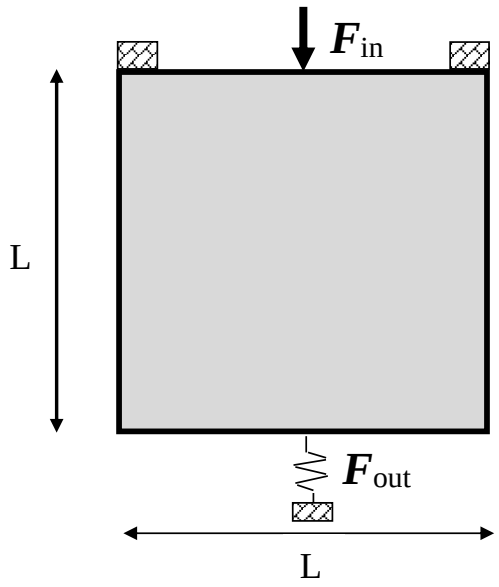

Fig. 9: Design domain for the mechanical inverter.

to compliance and volume constraints. We impose compliance constraints to prevent overly compliant designs. The optimization problem is stated as

$$\begin{aligned} &\min_{\boldsymbol{\rho}} \ \mu(Q_{MA}) \\ &\text{subject to } \mathbb{E}(V(\boldsymbol{\rho})) \leq 0.2, \\ &\qquad \mu(\boldsymbol{F}_{in}^T \boldsymbol{u}) + \lambda\sigma(\boldsymbol{F}_{in}^T \boldsymbol{u}) \leq \bar{C}_1, \\ &\qquad \mu(\boldsymbol{F}_{out}^T \boldsymbol{u}) + \lambda\sigma(\boldsymbol{F}_{out}^T \boldsymbol{u}) \leq \bar{C}_2, \\ &\qquad 0 \leq \boldsymbol{\rho} \leq 1. \end{aligned} \tag{30}$$

where μ and σ are the mean and standard deviation of the mechanical advantage $Q_{MA} = F_{out}/|F_{in}|$, and the compliance upperbounds are set to $\bar{C}_1 = 7.5 \times 10^4 \ N \cdot m$ and $\bar{C}_2 = 1.91 \times 10^5 \ N \cdot m$. The half domain is discretized with 48×96 quadrilateral isotropic finite elements.

Figure 10 shows the optimized design for lambda values $\lambda = 0.1$, $\lambda = 0.5$ and $\lambda = 1$. Similarly to previous example we generate a deterministic design (DET) which has a volume and compliance that is almost equal to that of the robust design (RDO) with $\lambda = 0.1$. These designs are shown in Figure 11. Table 3 compares the performance of the two designs, again showing the superiority of the RDO design. More precisely, the objective in this compliant mechanism example was to maximize the mean of mechanical advantage subject to constraining the mean and variance of compliance to ensure enough stiffness in the structure. Again, the RDO exhibits larger mean for the mechanical advantage and smaller robust criteria i.e. $\mu + \lambda\sigma$ for the compliance. This result indicates that the RDO design has higher capability in motion transfer yet is more stiff in the presence of uncertainty compared to the DET design which does not consider the scatter in the elastic moduli.

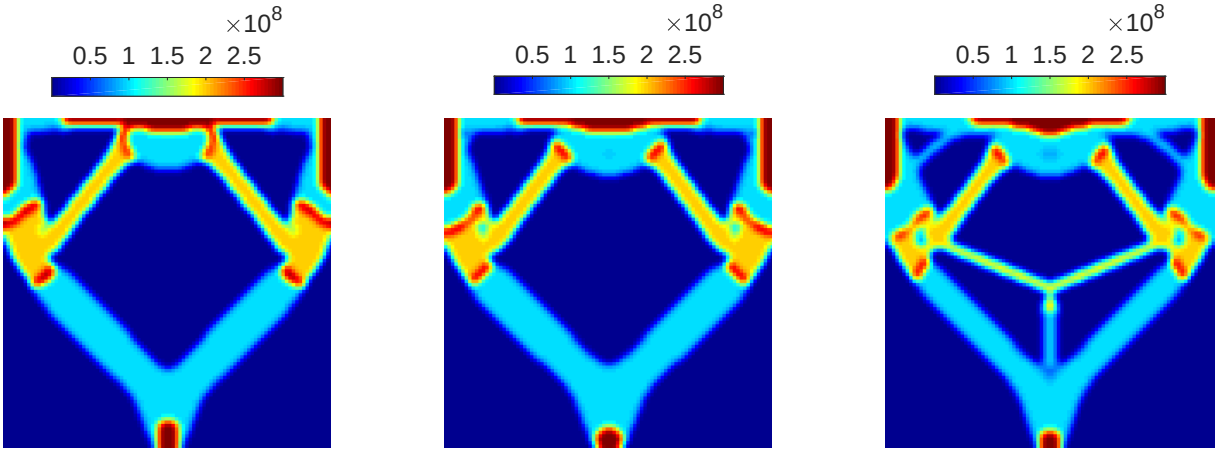

Fig. 10: Optimized material distribution for the mechanical inverter associated with $\lambda = 0.1$ (left), $\lambda = 0.5$ (middle) and $\lambda = 1$ (right).

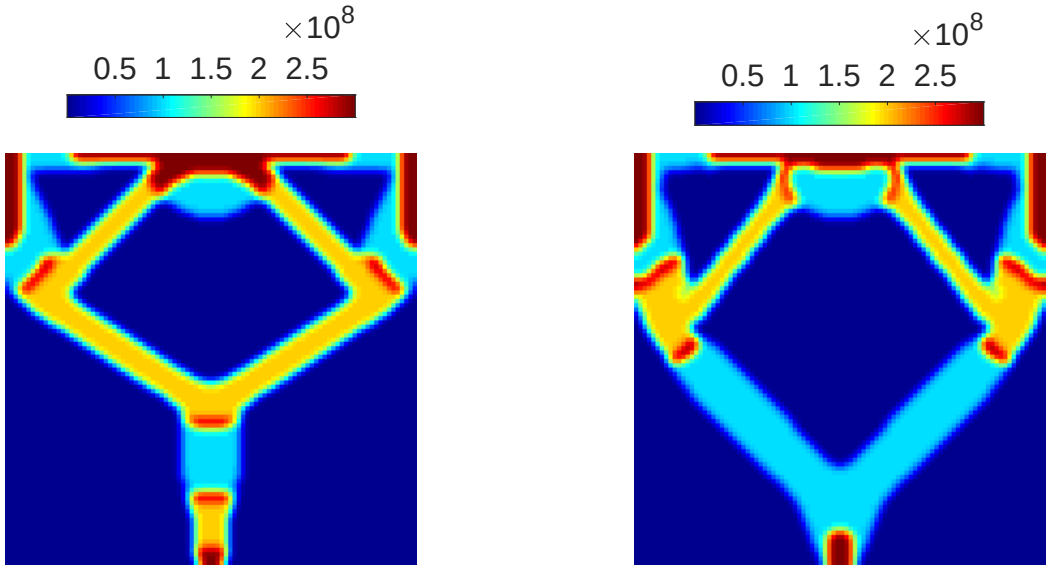

Fig. 11: Topology designs for the mechanical inverter: DET (left), RDO (right).

Table 3: Performance comparison between robust and deterministic designs with $\lambda = 0.1$ for mechanical inverter.

	$\mu(\boldsymbol{F}_{in}^T\boldsymbol{u}) + \lambda\sigma(\boldsymbol{F}_{in}^T\boldsymbol{u})$	$\mu(\boldsymbol{F}_{out}^T\boldsymbol{u}) + \lambda\sigma(\boldsymbol{F}_{out}^T\boldsymbol{u})$	$\mathbb{E}(V)$	$\mu(Q_{MA})$
DET	6.11×10^4	5.94×10^4	0.2012	0.473
RDO	7.49×10^4	4.46×10^4	0.2000	0.644

To better investigate the behavior of the optimization procedure in these designs, we show the convergence history of the stochastic quantities i.e. $\mu(\boldsymbol{F}_{in}^T\boldsymbol{u}) + \lambda\sigma(\boldsymbol{F}_{in}^T\boldsymbol{u}), \mu(\boldsymbol{F}_{out}^T\boldsymbol{u}) + \lambda\sigma(\boldsymbol{F}_{our}^T\boldsymbol{u}), \mathbb{E}(V)$ and $\mu(Q_{MA})$ evaluated for design

iterates of the RDO and DET designs in Figure 12. It is observed that while both designs exhibit convergence, the DET iterations result in a less optimal value for the mechanical advantage.

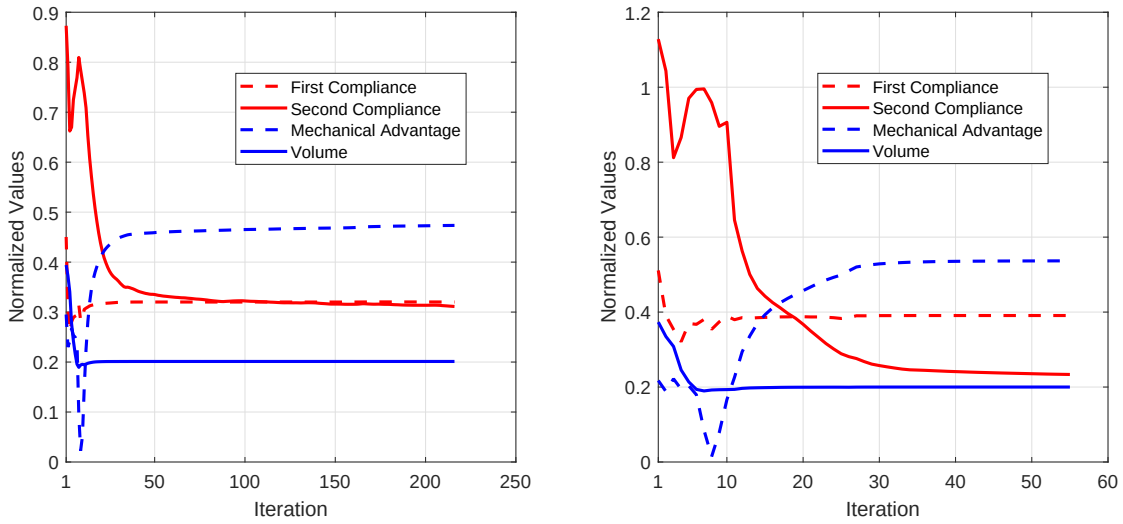

Fig. 12: Convergences histories of the stochastic quantities for the mechanical inverter optimization: DET (left), RDO (right).

4.3 Heat Sink Design

The objective in this example is to design a robust heat sink which minimizes the thermal compliance i.e. maximize the heat transfer within the domain shown in Figure 13. The governing equation and boundary conditions for a steady state

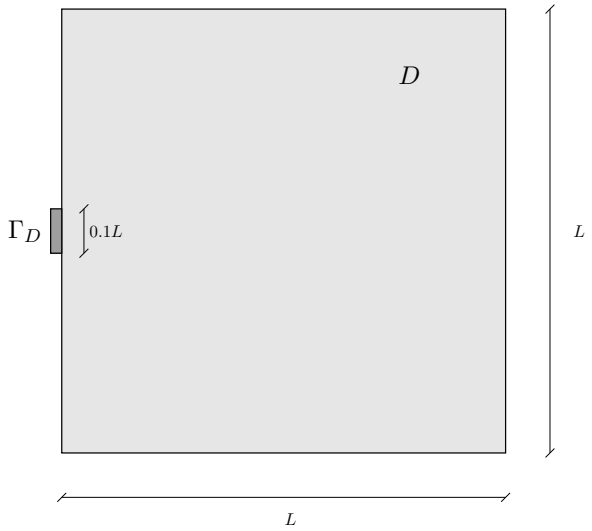

Fig. 13: Design domain for the heat sink. A zero temperature is imposed at the boundary Γ_D.

heat conduction problem are

$$\begin{cases} \nabla.\boldsymbol{q}(\boldsymbol{x}) + \mathbf{b}(\boldsymbol{x}) = 0 & \forall \boldsymbol{x} \in D \\ T(\boldsymbol{x}) = 0 & \forall \boldsymbol{x} \in \Gamma_D, \end{cases} \tag{31}$$

where $\boldsymbol{q}$ is the thermal flux and T is the temperature. Similarly to Equation (3), the elliptic PDE associated with Equation (31) is expressed as

$$\begin{cases} -\nabla.(\mathbb{K}(\boldsymbol{x})\nabla T(\boldsymbol{x})) = f(\boldsymbol{x}) & \forall \boldsymbol{x} \in D \\ T(\boldsymbol{x}) = 0 & \forall \boldsymbol{x} \in \partial D, \end{cases} \tag{32}$$

where $\mathbb{K}$ is the thermal conductivity matrix and $f(\boldsymbol{x})$ is the force function. After finite element discretization, the temperature $\boldsymbol{T} \equiv T(\boldsymbol{x})$ is obtained from $\boldsymbol{K}\boldsymbol{T} = \boldsymbol{F}$ where

$$\begin{aligned} \boldsymbol{K} &= \int_D \boldsymbol{B}^T \mathbb{K} \boldsymbol{B} dD \\ \boldsymbol{F} &= \int_D \boldsymbol{N}^T f dD \end{aligned} \tag{33}$$

are thermal stiffness matrix and thermal load vector, with $\boldsymbol{N}$ and $\boldsymbol{B}$ shape function matrix and its corresponding derivative matrix respectively. The thermal conductivity matrix $\mathbb{K}$ in this case is given by

$$\mathbb{K} = \mathcal{K}(\boldsymbol{\rho})\boldsymbol{I}_2, \tag{34}$$

where $\boldsymbol{I}_2$ is a 2×2 identity matrix and $\mathcal{K}(\boldsymbol{\rho})$ is the effective thermal conductance parameterized with respect to ρ_1 and ρ_2 at each element similarly to effective elastic modulus as described in Section 3.1.

We now solve a similar optimization problem to the first numerical example cf. Equation (29) where we use $C(\boldsymbol{\rho}) = \boldsymbol{T}^T\boldsymbol{F}$ as the thermal compliance. We use the same numerical values for nominal thermal conductance as the previous examples i.e. $\mathcal{K}_1^0 = 100\ W/(m \cdot K)$, $\mathcal{K}_2^0 = 200\ W/(m \cdot K)$, $\mathcal{K}_3^0 = 300\ W/(m \cdot K)$, $\mathcal{K}_{void} = 10^{-6}\ W/(m \cdot K)$ where $W/(m \cdot K)$ denotes watts per meter-kelvin, with a perturbation of $\delta = 0.05$ to introduce uncertainty. We use a finite element mesh containing 80×80 quadrilateral isotropic elements to discretize the design domain. Figure 14 shows the robust heat sink designs for different λ values. It is again observed that the most conductive material is placed in the regions with concentrated thermal load.

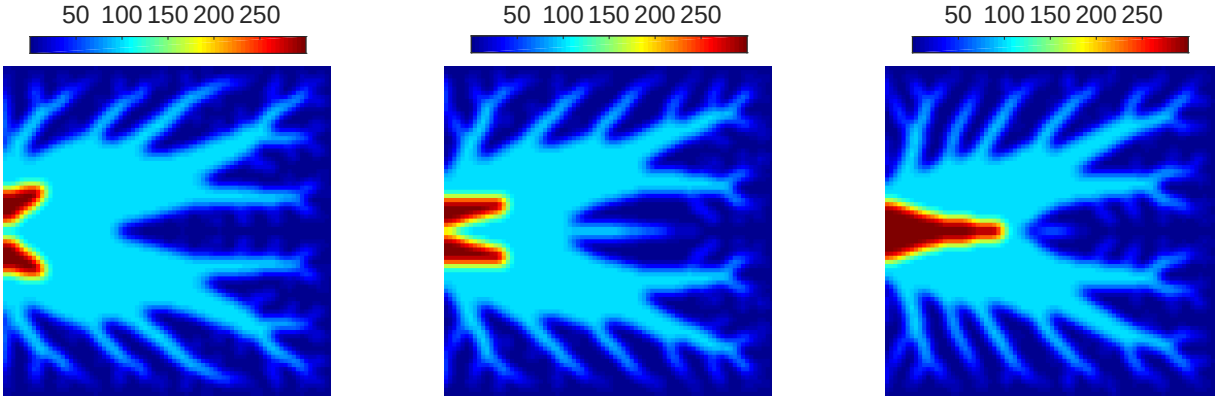

Fig. 14: Optimized material distributions for heat sink design associated with $\lambda = 0.1$ (left), $\lambda = 0.5$ (middle) and $\lambda = 1$ (right). The numbers on the color bar indicate the effective nominal thermal conductivity $\mathcal{K}^0$ (in $W/(m \cdot K)$) at each finite element.

Similarly to previous examples, we compare DET and RDO (with $\lambda = 1$) designs. Figures 15 and 16 show the optimized design and temperature field for DET and RDO designs. We use the nominal heat conduction values to compute

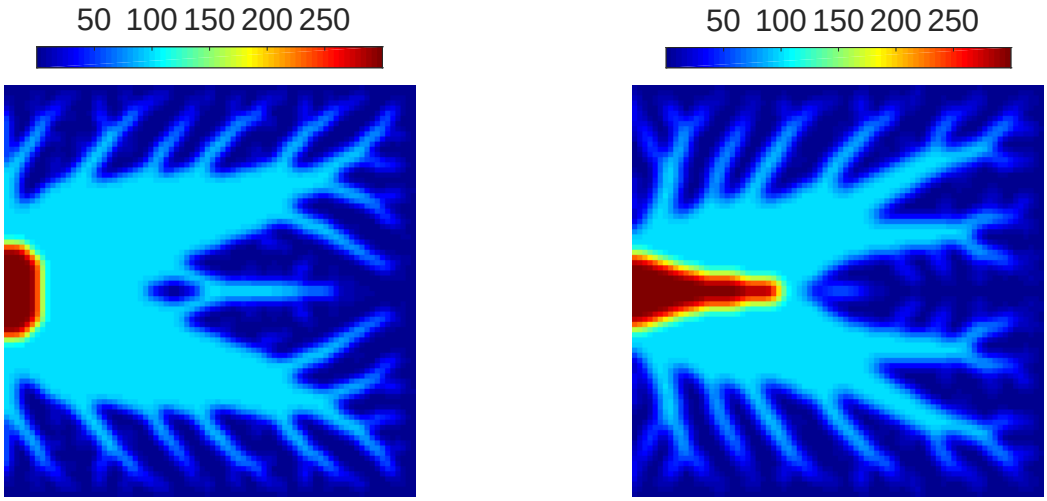

Fig. 15: Topology designs for the optimized heat sink: DET (left), RDO (right).

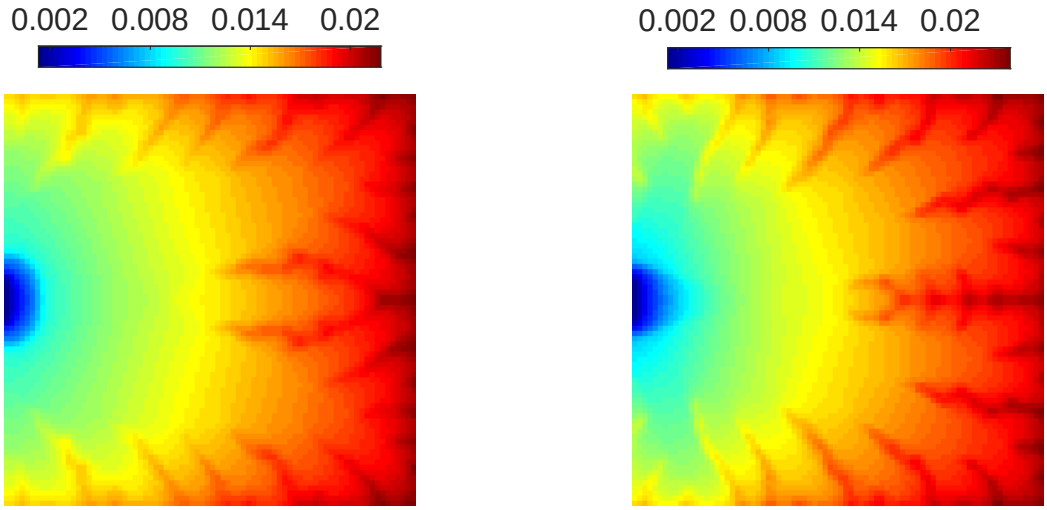

Fig. 16: Temperature distribution for optimized heat sink designs: DET (left), RDO (right). The numbers on the color bar indicate the temperature T (in kelvin) evaluated at the centroid of each element.

temperature in the RDO case. Similar to the structural topologies, the temperature distributions are visually distinguishable between RDO and DET cases.

The performance metrics for the two designs are listed in Table 4. The results show that the RDO design achieves a smaller thermal compliance which is in accordance with findings from previous examples.

Table 4: Performance comparison between the robust and deterministic designs with $\lambda = 1$ for heat sink.

	$\mu\ (W \cdot m \cdot K)$	$\sigma\ (W \cdot m \cdot K)$	$\mu + \lambda\sigma\ (W \cdot m \cdot K)$	$\mathbb{E}(V)$
DET	6.64×10^{-3}	5.88×10^{-3}	1.25×10^{-2}	0.30
RDO	6.32×10^{-3}	5.09×10^{-3}	1.14×10^{-2}	0.30

5 Conclusion

We have presented a systematic approach for multiphase topology optimization under uncertainty. The uncertainty in the design is motivated by the scatter in the material properties of candidate materials that are used in additive manufacturing processes. The optimization problem determines the optimal material at each spatial point in the domain. The robust design formulation ensures the optimal performance of the design in the presence of uncertainty. We have performed uncertainty analysis based on the well-established stochastic collocation approach, which involves simulations on collocation points in the domain of uncertain parameters. We used a novel quadrature strategy to alleviate the costly uncertainty analysis. We demonstrated our approach via numerical examples on linear elastic structures and a heat conduction problem. It is shown that robust designs which consider the scatter in material properties have improved performance when compared to designs obtained using standard deterministic methods.

The uncertainty in the local material properties reflects the inherent variability of the additive manufacturing process, in which multiple parameters can impact the effective properties of the printed parts. This parameters include, for example fluctuations in the velocity of the laser scan, variations in the radii of the powder particles (in powder-based AM technologies), and variability in the material's diffusion and absorption coefficients, each of which can introduce uncertainty in the manufacturing process [22]. The multimaterial robust design method presented in this paper, addresses this uncertainty in a systematic and mathematically rigorous way, thereby reducing variance in the performance of the optimized designs.

Appendix

The quadrature rule given in Table 5 is used throughout the numerical simulations for computing the statistical moments and their sensitivities.

Table 5: Designed nodes and weights for standard normal weight function associated with $d = 3, r = 6$.

y_1	y_2	y_3	w
0.171641741458233	0.689957250028694	-2.48133797897723	0.0195652215835242
-1.69315430845321	1.61708863138105	0.298045083369213	0.0300476893679597
3.92694274376759	-0.933214604741811	0.562757367213504	0.00145335874538015
1.34410141989722	0.381970662016496	2.91820733703388	0.00590909009609407
-2.31996570653233	-1.62281735871546	-1.25858957276265	0.00651299744901662
-0.630213024184360	3.05972970814128	-1.39953690170700	0.00319568555246638
-0.739813154711971	-2.20948987153464	0.282366525038571	0.0321695273195095
-0.768638770177116	-1.01481585040187	1.98744088127226	0.0300476893664722
2.70348703623727	2.54971069685634	-1.67290103514329	0.00145335874524301
-0.421120916190286	-0.344301814355217	-0.305929882386066	0.267761767987068
1.28213840842346	-2.38433920975212	2.09496193629465	0.00319568555398788
-2.21217043808382	-0.353010684943172	0.660647754050324	0.0333400972163237
-1.71481025764031	0.566125181577248	-1.49927579511206	0.0321695273198626
-0.371357624149492	0.773077117006202	1.40759851883070	0.102793002755931
-4.39569861562540	2.62707460199759	6.49824103052430	1.94327102374642e-05
1.58701997262256	-0.206417759980910	-1.19006833946956	0.0642371018551073
0.966978796119146	-0.721732490252721	0.769074015073605	0.129575133876131
1.18852859905139	-2.20490926878007	-0.623149216331885	0.0195652215841040
1.69943159998911	0.987820543619816	0.608914972296741	0.0524740241189448
0.255442476607422	1.30386421492425	-0.531138278217719	0.129575133874885
0.445753032850931	2.93938267731708	1.27662758285290	0.00590909009647187
-0.193161917553007	-1.33369752229607	-1.97205610209462	0.0290301628252801

Acknowledgements

The authors wish to acknowledge the support of the National Science Foundation, which funded this research through grant number CMMI-1663566.

Conflict of Interest

All authors hereby declare that there is no conflict of interest.

Replication of Results

For readers seeking to replicate the results presented in this paper, the MATLAB scripts for computing the quantities of interest, namely compliance, volume and mechanical advantage, as well as statistical moments and their associated sensitivities corresponding to three numerical examples are provided in the public repository linked to in reference [37]. The data associated with the new quadrature rule, which is used for computation of statistical moments and their sensitivities, are also provided in this repository.

References

1. MP Bendsøe and N. Kikuchi. Generating optimal topologies in structural design using a homogenization method. *Computer Methods in Applied Mechanics and Engineering*, 71(2):197 – 224, 1988.
2. O. Sigmund and S. Torquato. Design of materials with extreme thermal expansion using a three-phase topology optimization method. *Journal of the Mechanics and Physics of Solids*, 45(6):1037 – 1067, 1997.
3. Joe Alexandersen, Ole Sigmund, Knud Erik Meyer, and Boyan Stefanov Lazarov. Design of passive coolers for light-emitting diode lamps using topology optimisation. *International Journal of Heat and Mass Transfer*, 122:138 – 149, 2018.
4. Qing Li, Grant P. Steven, Osvaldo M. Querin, and Y.M. Xie. Shape and topology design for heat conduction by evolutionary structural optimization. *International Journal of Heat and Mass Transfer*, 42(17):3361 – 3371, 1999.
5. Sumer B. Dilgen, Cetin B. Dilgen, David R. Fuhrman, Ole Sigmund, and Boyan S. Lazarov. Density based topology optimization of turbulent flow heat transfer systems. *Structural and Multidisciplinary Optimization*, 57(5):1905–1918, May 2018.
6. Christian Lundgaard and Ole Sigmund. A density-based topology optimization methodology for thermoelectric energy conversion problems. *Structural and Multidisciplinary Optimization*, 57(4):1427–1442, Apr 2018.
7. Reza Behrou and Kurt Maute. Multiscale modeling of non-local damage evolution in lithium-ion batteries. *ECS Transactions*, 77(11):1163–1177, 2017.
8. Reza Behrou, Matthew Lawry, and Kurt Maute. Level set topology optimization of structural problems with interface cohesion. *International Journal for Numerical Methods in Engineering*, 112(8):990–1016.
9. J.K. Guest and M. Zhu. Casting and milling restrictions in topology optimization via projection-based algorithms. In *ASME 2012 International Design Engineering Technical Conferences and Computers and Information in Engineering Conference*.
10. S.L. Vatanabe, T.N. Lippi, C.R. de Lima, G.H. Paulino, and E.C.N. Silva. Topology optimization with manufacturing constraints: A unified projection-based approach. *Advances in Engineering Software*, 100:87–112, 2016.
11. Jikai Liu, Andrew T. Gaynor, Shikui Chen, Zhan Kang, Krishnan Suresh, Akihiro Takezawa, Lei Li, Junji Kato, Jinyuan Tang, Charlie C. Wang, Lin Cheng, Xuan Liang, and Albert. C. To. Current and future trends in topology optimization for additive manufacturing. *Struct. Multidiscip. Optim.*, 57(6):2457–2483, June 2018.
12. Tomás Zegard and Glaucio H. Paulino. Bridging topology optimization and additive manufacturing. *Struct. Multidiscip. Optim.*, 53(1):175–192, January 2016.
13. M. Leary, L. Merli, F. Torti, M. Mazur, and M. Brandt. Optimal topology for additive manufacture: A method for enabling additive manufacture of support-free optimal structures. *Materials & Design*, 63:678690, 2014.
14. D. Brackett, I. Ashcroft, and R. Hague. Topology optimization for additive manufacturing.
15. Y. Mass and O. Amir. Topology optimization for additive manufacturing: Accounting for overhang limitations using a virtual skeleton. *Additive Manufacturing*, 18:58–73, 2017.

16. Andrew T. Gaynor and James K. Guest. Topology optimization considering overhang constraints: Eliminating sacrificial support material in additive manufacturing through design. *Struct. Multidiscip. Optim.*, 54(5):1157–1172, November 2016.
17. M. Langelaar. An additive manufacturing filter for topology optimization of print-ready designs. *Structural and Multidisciplinary Optimization*, 55:871–883, 2016.
18. M. Langelaar. Topology optimization of 3d self-supporting structures for additive manufacturing. *Additive Manufacturing*, 12A:60–70, 2017.
19. X. Qian. Undercut and overhang angle control in topology optimization: a density gradient based integral approach. *Interntional Journal for Numerical Methods in Engineering*, 111:247272, 2017.
20. A.T. Gaynor, N.A. Meisel, C.B. Williams, and J.K. Guest. Multiple-material topology optimization of compliant mechanisms created via Polyjet three-dimensional printing. *Journal of Manufacturing Science and Engineering*, 136:1–10, 2014.
21. Cian Conlan-Smith, Anurag Bhattacharyya, and Kai A. James. Optimal design of compliant mechanisms using functionally graded materials. *Structural and Multidisciplinary Optimization*, 57(1):197–212, jul 2017.
22. Zhen Hu and Sankaran Mahadevan. Uncertainty quantification in prediction of material properties during additive manufacturing (viewpoint paper). *Scripta Materialia*, 135(C):135–140, 2017.
23. MP Bendsøe and N. Kikuchi. Robust shape optimization of continuous structures via the level set method. *Computer Methods in Applied Mechanics and Engineering*, 305:271 – 291, 2016.
24. F De Gournay, G Allaire, and F. Jouve. Shape and topology optimization of the robust compliance via the level set method. *ESAIM: COCV*, 1:43 – 70, 2008.
25. Vahid Keshavarzzadeh, Hadi Meidani, and Daniel A. Tortorelli. Gradient based design optimization under uncertainty via stochastic expansion methods. *Computer Methods in Applied Mechanics and Engineering*, 306:47 – 76, 2016.
26. Vahid Keshavarzzadeh, Felipe Fernandez, and Daniel A. Tortorelli. Topology optimization under uncertainty via non-intrusive polynomial chaos expansion. *Computer Methods in Applied Mechanics and Engineering*, 318:120 – 147, 2017.
27. A. J. Torii, R. H. Lopez, and L. F. F. Miguel. A gradient-based polynomial chaos approach for risk and reliability-based design optimization. *Journal of the Brazilian Society of Mechanical Sciences and Engineering*, 39(7):2905–2915, Jul 2017.
28. Jesus Martinez-Frutos, David Herrero-Perez, Mathieu Kessler, and Francisco Periago. Risk-averse structural topology optimization under random fields using stochastic expansion methods. *Computer Methods in Applied Mechanics and Engineering*, 330:180 – 206, 2018.
29. D. Xiu and J. Hesthaven. High-order collocation methods for differential equations with random inputs. *SIAM Journal on Scientific Computing*, 27(3):1118–1139, 2005.
30. Boyan S. Lazarov, Mattias Schevenels, and Ole Sigmund. Topology optimization considering material and geometric uncertainties using stochastic collocation methods. *Structural and Multidisciplinary Optimization*, 46(4):597–612, Oct 2012.
31. V. Keshavarzzadeh, Robert M. Kirby, and A. Narayan. Numerical integration in multiple dimensions with designed quadrature. *SIAM Journal on Scientific Computing*, 40(4):A2033–A2061, 2018.
32. Xu Guo, Xiaofang Zhao, Weisheng Zhang, Jun Yan, and Guomin Sun. Multi-scale robust design and optimization considering load uncertainties. *Computer Methods in Applied Mechanics and Engineering*, 283:994 – 1009, 2015.
33. Seyyed Ali Rostami and Ali Ghoddosian. Topology optimization of continuum structures under hybrid uncertainties. *Struct. Multidiscip. Optim.*, 57(6):2399–2409, June 2018.
34. Jess Martnez-Frutos and David Herrero-Prez. Evolutionary topology optimization of continuum structures under uncertainty using sensitivity analysis and smooth boundary representation. *Computers & Structures*, 205:15 – 27, 2018.
35. Qinghai Zhao, Xiaokai Chen, Zheng-Dong Ma, and Yi Lin. Robust topology optimization based on stochastic collocation methods under loading uncertainties. *Mathematical Problems in Engineering*, 2015.
36. Kohei Shintani, Yu-Chin Chan, and Wei Chen. Robust multi-material topology optimization for lattice structure under material uncertainties. *Advances in Structural and Multidisciplinary Optimization. WCSMO 2017*, pages 1110–1123.
37. Vahid Keshavarzzadeh and Kai A. James. Numerical implementation for robust multiphase topology optimization. `http://github.com/vahid28k/TOPOPT-RTO-MM`.
38. Krister Svanberg. The method of moving asymptotes-a new method for structural optimization. *International Journal for Numerical Methods in Engineering*, 24(2):359–373, 1987.

39. Erik Andreassen, Anders Clausen, Mattias Schevenels, Boyan S. Lazarov, and Ole Sigmund. Efficient topology optimization in matlab using 88 lines of code. *Structural and Multidisciplinary Optimization*, 43(1):1–16, Jan 2011.
40. Kai A. James. Multiphase topology design with optimal material selection using an inverse p-norm function. *International Journal for Numerical Methods in Engineering*, 114(9):999–1017, 2018.
41. TE Bruns and DA. Tortorelli. Topology optimization of non-linear elastic structures and compliant mechanisms. *Computer Methods in Applied Mechanics and Engineering*, 190(26-27):3443 – 3459, 2001.
42. J. K. Guest, J. H. Prevost, and T. Belytschko. Achieving minimum length scale in topology optimization using nodal design variables and projection functions. *International Journal for Numerical Methods in Engineering*, 61(2):238–254, 2004.
43. MP. Bendsøe. Optimal shape design as a material distribution problem. *Structural optimization*, 1(4):193–202, 1989.
44. MP Bendsøe and O. Sigmund. Material interpolation schemes in topology optimization. *Archive of Applied Mechanics*, 69(9):635–654, 1999.
45. F. Heiss and V. Winschel. Likelihood approximation by numerical integration on sparse grids. *Journal of Econometrics*, 144(1):62 – 80, 2008.
46. F Heiss and V. Winschel. Quadrature on sparse grids. `http://www.sparse-grids.de/`.
47. D. A. Tortorelli and P. Michaleris. Design sensitivity analysis: Overview and review. *Inverse Problems in Engineering*, 1(1):71–105, 1994.
48. Roger G. Ghanem. The nonlinear gaussian spectrum of log-normal stochastic processes and variables. *ASME. J. Appl. Mech.*, 66(4):964–973, 1999.
49. Chau Le, Julian Norato, Tyler Bruns, Christopher Ha, and Daniel Tortorelli. Stress-based topology optimization for continua. *Structural and Multidisciplinary Optimization*, 41(4):605–620, Apr 2010.
50. RG Ghanem and PD Spanos. Stochastic finite elements: A spectral approach. *Dover publications*, 2002.
51. D. Xiu and G. Karniadakis. The wiener–askey polynomial chaos for stochastic differential equations. *SIAM Journal on Scientific Computing*, 24(2):619–644, 2002.